Physics-Informed Filtering for Ultrasonic Guided Wave Structural Health Monitoring

JOEL B. HARLEY, AMANDA BECK, WOOHYUN EUM,
MICHAEL MACISSAC, CHARLIE TRAN and GHATU SUBHASH

ABSTRACT

This paper presents a methodology for physics-informed filtering, applied to ultrasonic guided waves. The physics-informed filters are derived by integrating physics-based constraints into an optimization framework, where the cost function comprises of two components: a reconstruction error term and a regularization term. The reconstruction error term ensures the filtered data closely aligns with the original measurements while the regularization term enforces physical laws represented by a linear operator. We derive a general closed-form solution for these filters and then apply them with the two-dimensional Helmholtz equation. We apply these filters, using various parameters, to ultrasonic guided wave data collected by a laser Doppler vibrometer. We demonstrate the ability to characterize damage regions with thickness losses from the filtered data.

INTRODUCTION

Use of physics-informed learning and physics-informed neural networks has grown in structural health monitoring to integrate physics principles with flexible deep learning algorithms [1–4]. In these scenarios, physical principles often foundationally ground the traditionally black-box deep learning algorithms, improving the robustness of analyses and increasing interpretability / trust [5]. These approaches can also be used as a much faster replacement for traditional computational modeling solutions [6]. Recently, it has been shown that we can learn shallow, linear optimal filters that fi t data to linear partial differential equations (such as the Helmholtz equation) [7–9]. This perspective is valuable for applications in structural health monitoring, where we analyze solutions to linear partial differential equations, and the human interpretability of our data analytics is important to ensure the safety of our structures.

This paper focuses on studying shallow physics-informed filters, their relationship to structural health monitoring (with a focus on guided waves), and how they can be used to improve the analysis of guided wave data. The physics-informed filter removes and/or retains components of the data that satisfy particular physical parameters. This is analogous to traditional signal processing applications, where we aim to remove or re-

Joel B. Harley, email: joel.harley@ufl.edu. SmartData Lab, Department of Electrical and Computer Engineering, University of Florida, Gainesville, FL, USA

tain specific frequencies rather than specific physical parameters. However, the physics-informed filter can be customized for many different physical scenarios. Unlike advances in physics-informed neural networks [10], this approach is not inherently a machine learning tool but is designed for more general data analytics. Also, while physics-informed neural networks constrain solutions to physical solutions, they do not provide physically interpretable explanations for their solutions. Physics-informed filters help bridge this interpretability gap.

In this paper, we specifically explore Helmholtz filters, which are constrained by the Helmholtz equation. We demonstrate that these filters have a physically elegant interpretation and retain only the data fitting the wavenumber parameter in the Helmholtz equation while removing all others. We demonstrate how to choose and modify the center wavenumber and its bandwidth. Note that this approach is not entirely different from existing wavenumber filtering approaches in the literature [11–14] but provides a more rigorous mathematical foundation for them. We apply Helmholtz filtering to ultrasonic guided wave wavefield data of an aluminum plate with heterogeneous thickness losses. We show that these filters can be used to characterize damage / thickness variations and learn the frequency-wavenumber dispersion relationships.

PHYSICS-INFORMED FILTERS

We will consider a single-mode physics-informed filter defined by a homogeneous, linear equation. We will refer to this filter as single-mode since the data is assumed to be composed of a single solution to the physics. Multi-mode data would be composed of a sum of multiple solutions (with different parameters) to a single physics equation.

Definition

We can derive the physics-informed filter as the solution to an optimization problem

$$\min_{\mathbf{y}} f(\mathbf{x}, \mathbf{y}, \boldsymbol{\theta}, \mathbf{P}) \tag{1}$$

where the cost function is related to the data $\mathbf{x}$, filtered representation $\mathbf{y}$, the linear physics operator $\mathbf{P}$, and the parameters of that physics operator $\boldsymbol{\theta}$. The general cost function can then be expressed as

$$f(\mathbf{x}, \mathbf{y}, \boldsymbol{\theta}, \mathbf{P}) = \|\mathbf{x} - \mathbf{y}\|_2^2 + \frac{1}{\gamma^2} \|\mathbf{P}_{\boldsymbol{\theta}} \mathbf{y}\|_2^2 \ . \tag{2}$$

This cost function has two terms. The first term aims to identify a filtered representation $\mathbf{y}$ that is optimally close to the provided data. The second term aims to enforce linear physics on the filtered representation $\mathbf{y}$, as defined by a linear operator $\mathbf{P}_{\boldsymbol{\theta}}$. The term γ^2 represents the weight given to the physics.

The general solution to this problem can be identified in closed form by taking the derivative of the cost function with respect to $\mathbf{y}$, setting the derivative to zero, and solving for $\mathbf{y}$. Specifically, differentiating the cost function to find the minimum yields

$$\frac{df(\mathbf{x}, \mathbf{y}, \boldsymbol{\theta}, \mathbf{P})}{d\mathbf{y}} = -2\mathbf{x} + 2\mathbf{y} + 2\frac{1}{\gamma^2} \mathbf{P}_{\boldsymbol{\theta}}^H \mathbf{P}_{\boldsymbol{\theta}} \mathbf{y} = 0 \ . \tag{3}$$

Therefore, the solution to the physics-informed, single-mode optimization problem is

$$\mathbf{y} = \left(\mathbf{I} + \frac{1}{\gamma^2}\mathbf{P}_{\boldsymbol{\theta}}^H \mathbf{P}_{\boldsymbol{\theta}}\right)^{-1} \mathbf{x} \, . \tag{4}$$

Hence, solving this matrix inverse problem will learn a vector that optimally aims to match both the provided data and the physics.

Spectral Representation of Physics-Informed Filters

A significant challenge with this formulation is that we may be required to compute the inverse of very large matrices across multiple dimensions, which can be computationally intractable. This can be addressed by diagonalizing our physics operator.

Specifically, if we diagonalize $\mathbf{P}_{\boldsymbol{\theta}}$ with the singular value decomposition, we get

$$\mathbf{P}_{\boldsymbol{\theta}} = \mathbf{U}_{\boldsymbol{\theta}} \boldsymbol{\Lambda}_{\boldsymbol{\theta}} \mathbf{V}_{\boldsymbol{\theta}}^H \, . \tag{5}$$

When we plug this into the solution to the physics-informed filtering, we get

$$\mathbf{y} = \mathbf{V}_{\boldsymbol{\theta}} \left(\mathbf{I} + \frac{1}{\gamma^2}\boldsymbol{\Lambda}_{\boldsymbol{\theta}}^2\right)^{-1} \mathbf{V}_{\boldsymbol{\theta}}^H \mathbf{x} \qquad , \qquad \widehat{\mathbf{y}}_{\boldsymbol{\theta}} = \left(\mathbf{I} + \frac{1}{\gamma^2}\boldsymbol{\Lambda}_{\boldsymbol{\theta}}^2\right)^{-1} \widehat{\mathbf{x}}_{\boldsymbol{\theta}} \, . \tag{6}$$

In this expression, $\widehat{\mathbf{y}}_{\boldsymbol{\theta}}$ and $\widehat{\mathbf{x}}_{\boldsymbol{\theta}}$ are the filtered and original data in a new representation, often referred to as a spectral domain. With this diagonalization, we see that the solution is now achieved by taking the inverse of a diagonal matrix, significantly improving the computational cost.

If $\mathbf{P}_{\boldsymbol{\theta}}$ represents a linear differential equation, we can write the operator as

$$\mathbf{P}_{\boldsymbol{\theta}=\{\alpha_N,\ldots,\alpha_1,\alpha_0\}} = \alpha_N \mathbf{D}^N + \alpha_{N-1}\mathbf{D}^{N-1} + \cdots + \alpha_1 \mathbf{D} + \alpha_0 \, , \tag{7}$$

where $\mathbf{D}$ represents a derivative operator (or an approximate derivative operator for discrete data) and $\mathbf{D}^n$ represents the n-th derivative operator. The physics parameters θ then become the unknown of this differential equation.

If $\mathbf{D}$ is a matrix (i.e., a discrete approximation of the derivative) and defined to have a circulant structure (thereby assuming periodic boundary conditions), then the singular vectors of $\mathbf{P}_{\boldsymbol{\theta}}$ will always be a discrete Fourier transform matrix. Furthermore, under this condition, the singular vectors are no longer dependent on the coefficients θ, so $\mathbf{V}_\theta = \mathbf{V}$, $\widehat{\mathbf{y}}_\theta = \widehat{\mathbf{y}}$, and $\widehat{\mathbf{x}}_\theta = \widehat{\mathbf{x}}$. Therefore, $(\mathbf{I} + 1/\gamma^2 \boldsymbol{\Lambda}_{\boldsymbol{\theta}}^2)^{-1}$ represents our filter in the spectral domain, which is element-wise multiplied (due to the matrices being diagonal) by $\widehat{\mathbf{x}}$ (the spectral representation of the data) to get a filtered spectral representation $\widehat{\mathbf{y}}$.

We can transfer between domains by utilizing the transformations

$$\widehat{\mathbf{y}} = \mathbf{V}^H \mathbf{y} \qquad , \qquad \mathbf{y} = \mathbf{V}\widehat{\mathbf{y}} \, . \tag{8}$$

This allows us to return to the original representation after filtering the signal. Again, if our approximate derivative operators have periodic boundary conditions, then $\mathbf{V}^H$ corresponds to the discrete Fourier transform and $\mathbf{V}$ corresponds to the inverse discrete Fourier transform, quickly computable via the fast Fourier transform algorithm.

THE TWO-DIMENSIONAL HELMHOLTZ PHYSICS-INFORMED FILTER

In guided wave processing, the Helmholtz equation is of significant value since it represents the frequency-independent wave equation. At each frequency, guided waves can be represented as a collection of modes that each satisfy the Helmholtz equation. The two-dimensional Helmholtz equation with wavenumber $\widehat{k}$ can be expressed as

$$\frac{\partial^2 u(x,y)}{\partial x^2} + \frac{\partial^2 u(x,y)}{\partial y^2} + \widehat{k}^2 u(x,y) = 0 \tag{9}$$

where $\widehat{k} = \omega / c_0$ is the wavenumber, with chosen angular frequency ω and wave speed c_0.

The physics matrix for the two-dimensional Helmholtz equation can be expressed as

$$\mathbf{P}_{\widehat{k}} = \mathbf{I}_y \otimes \mathbf{D}_x^2 + \mathbf{D}_y^2 \otimes \mathbf{I}_x + \widehat{k}^2 \mathbf{I}_y \otimes \mathbf{I}_x \tag{10}$$

where $\mathbf{I}_y$ and $\mathbf{I}_x$ are identity matrices with sizes of N_y and N_x, respectively. In addition, $\mathbf{D}_x^2$ and $\mathbf{D}_y^2$ are second-derivative operators, discrete approximations of the second derivative operation, for their respective dimensions. Finally, $\otimes$ represents the Kronecker product operation. Note that while the data $\mathbf{x}$ is two-dimensional, we assume it has been vectorized (the columns of its matrix are stacked) before being multiplied by $\mathbf{P}_{\widehat{k}}$.

EXPERIMENTAL SETUP

To demonstrate Helmholtz filtering, guided wave data was collected from a 15.24 cm by 15.24 cm by 0.81 mm aluminum plate. Using a laser Doppler vibrometer sensing the backside of the plate, we measure an approximately 10 cm by 10 cm field of guided waves as they travel throughout the plate. The guided waves are transmitted from a piezoelectric transducer located 0.5 cm outside of the sensing region. The piezoelectric transmits a chirp pulse [15] that linearly increases from 0 kHz to 300 kHz in 0.5 ms, and the response is recorded for 1 ms. In roughly the center of the aluminum plate, we have used a Dremel tool to create a hole as well as a surrounding region of thickness loss.

From this dataset, Figure 1 illustrates three different representations of the data. Figure 1(a) shows our wavefield data in the spatial domain at a single point in time (at time $t = 0.3$ ms). Figure 1(b) shows our wavefield data in the spatial domain at a single frequency (at frequency 199 kHz). For reader clarity, the chirp signal travels from top to bottom. Figure 1(c) illustrates our wavefield data in the spatial frequency / spectral domain at a single frequency (at frequency 199 kHz). In the first two plots, we can observe a damaged region in roughly the center of the wavefield, characterized by higher amplitudes and smaller wavelengths. In the last plot, we observe a single strong ring representing the dominant wavenumber in the wavefield, at that frequency.

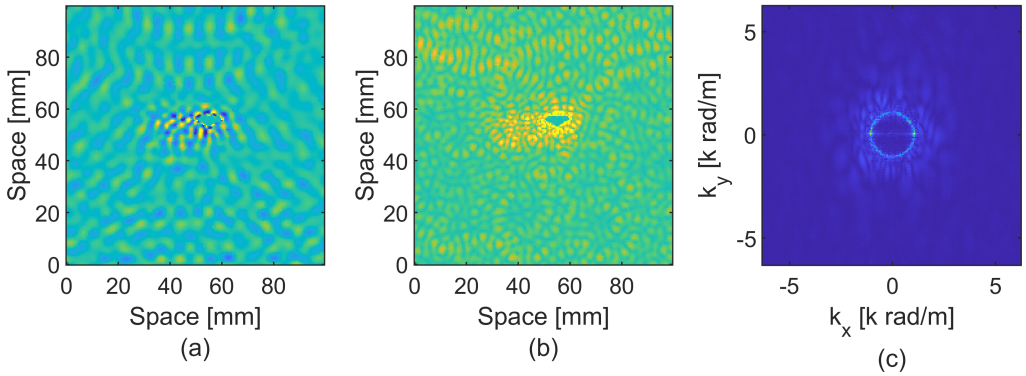

Figure 1. Illustration of our guided wave data (a) in the spatial domain at time $t = 0.1$ ms, (b) in the spatial domain at frequency 199 kHz, and (c) in the wavenumber domain at frequency 199 kHz.

RESULTS AND DISCUSSION

In this section, we apply our two-dimensional Helmholtz physics-informed filter to our guided wave data to demonstrate the information that can be extracted in this spectral / wavenumber domain. Through this process, we modify two variables: $\widehat{k}$ and γ^2. The value of $\widehat{k}$ corresponds to the center wavenumber for our Helmholtz filter, while the value of γ^2 corresponds to the bandwidth for our Helmholtz filter.

Two-Dimensional Helmholtz Filters

To demonstrate the capabilities of the two-dimensional Helmholtz filter, we choose a collection of $\widehat{k}$ values corresponding to different bands of the wavenumber domain. Specifically, we choose values of

$$\widehat{k}_n = 2n(\Delta k)\,. \tag{11}$$

Furthermore, we choose values of γ^2 to have an approximate equal wavenumber bandwidth of Δk. This is accomplished by choosing

$$\gamma_n^2 = (\Delta k)^4(4n+1)^2\,. \tag{12}$$

Hence, the value of changes with choice of $\widehat{k}_n$ to maintain a constant bandwidth of approximately Δk. Note that the bandwidth is not exactly Δk since the values are not perfectly symmetric around $\widehat{k}_n$.

Figure 2 shows the Helmholtz filters (top row), the associated filter spectral representations (middle row), and the associated filtered single-spatial representation (bottom) for our guided wave data at a frequency of 199 kHz. For these filters, we use a $\Delta k = 250$ rad/m and show $n = 1$ to $n = 6$. We can see that after applying the wavenumber filter, we observe a peak at the location of the hole since there are no waves there. The second filter obtains the thickest parts of the plate. As we increase the center wavenumber, we observe that we extract different regions (albeit with some overlap,

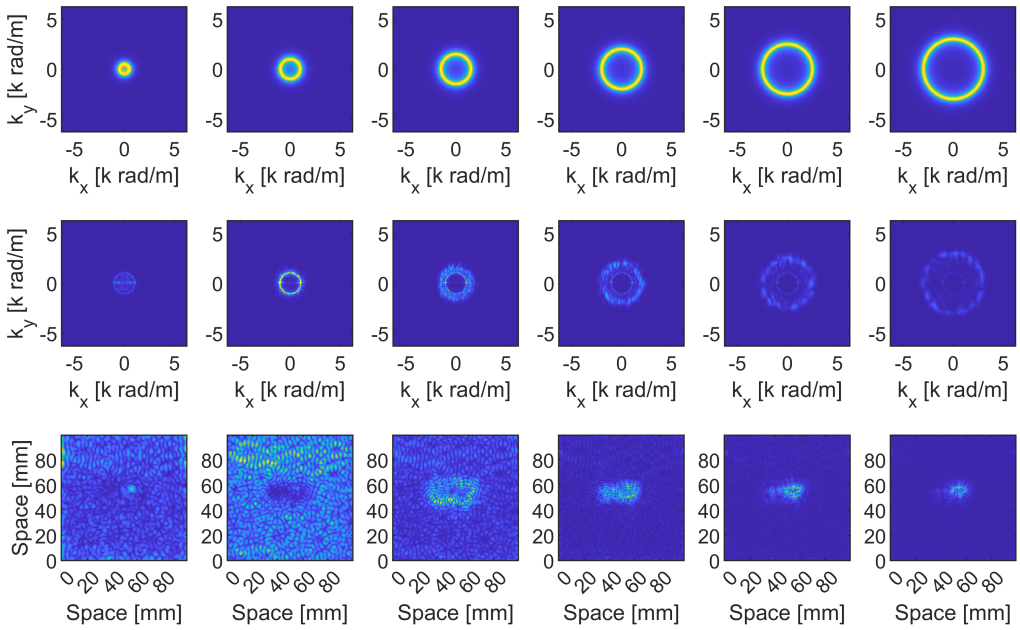

Figure 2. Illustration of (top) the filter in the wavenumber domain, (middle) the filtered guided wave data in the wavenumber domain at a single frequency of 199 kHz, and (bottom) the filtered guided wave data in the spatial domain at a single frequency of 199 kHz. From left to right, the filter values of k_n and γ_n^2 advance from $n = 1$ to $n = 6$ with $\Delta k = 250$ rad/m.

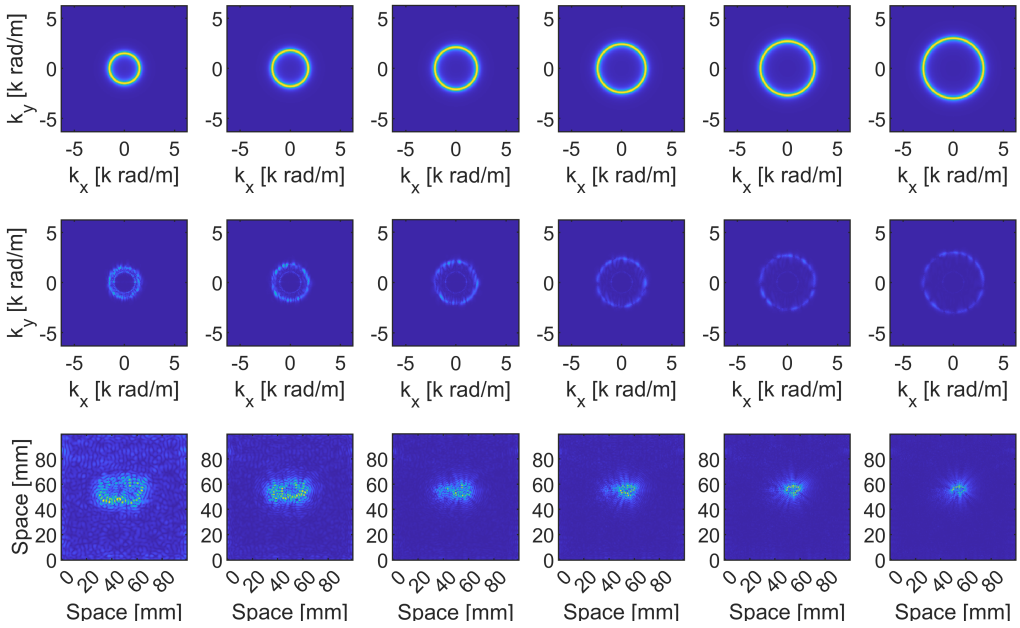

Figure 3. Illustration of (top) the filter in the wavenumber domain, (middle) the filtered guided wave data in the wavenumber domain at a single frequency of 199 kHz, and (bottom) the filtered guided wave data in the spatial domain at a single frequency of 199 kHz. From left to right, the filter values of k_n and γ_n^2 advance from $n = 5$ to $n = 10$ with $\Delta k = 150$ rad/m.

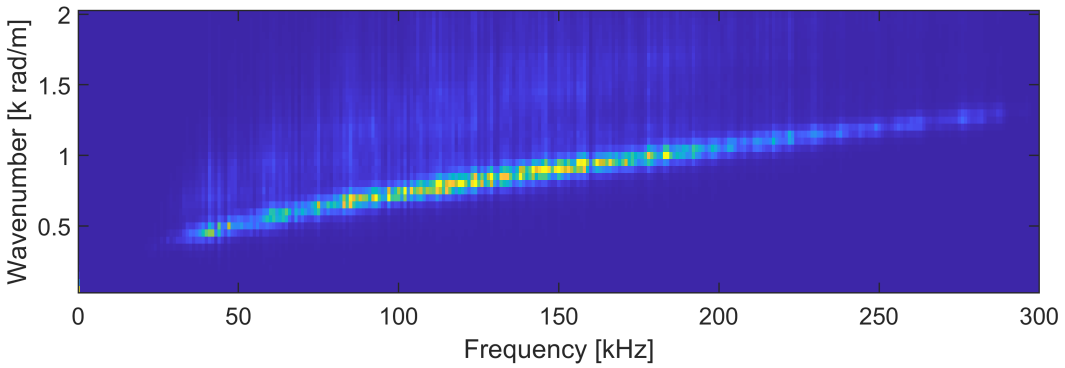

Figure 4. The squared sum of our filtered guided wave data at each wavenumber (defined by a the filter's $\widehat{k}$ value and frequency. The dominant curve is the Lamb wave zeroth antisymmetric mode.

likely due to wavelength resolutions at this frequency) corresponding to different thicknesses in the plate. Higher wavenumbers correspond to smaller thicknesses.

Figure 3 shows similar Helmholtz filter results for $\Delta k = 150$ rad/m and $n = 5$ to $n = 10$. This demonstrates that by reducing the bandwidth of the Helmholtz filter, we can obtain better spatial resolutions of the thickness changes in the aluminum plate.

Dispersion Curve Extraction

Figure 4 illustrates the results of applying these Helmholtz filters to frequencies from 0 kHz to 300 kHz and then plotting the squared sum of the filtered components. The results are plotted in the frequency-wavenumber domain. This is done for a choice of $\Delta k = 25$ rad/m. Figure 4 illustrates that this produces the dispersion curves for the wave. Specifically, we observe a dominant curve corresponding to the zeroth asymmetric mode. We then observe a weaker, more diffuse curve at higher wavenumbers. These values correspond to the wavenumbers / thicknesses of the damaged region. These results demonstrate how the Helmholtz filter can characterize materials.

CONCLUSIONS

In this paper, we developed a physics-informed data filtering approach based on integrating the two-dimensional Helmholtz equation into an optimization framework. Our method ensures the filtered data remains similar to the original measurements while adhering to known Helmholtz. We demonstrated that these filtering operations can be derived in a spectral domain, which reduces computational cost and increases interpretability / explainability of the filters / optimization framework. Our results demonstrate that different filters can extract different wavenumbers from the data and correspond to different thicknesses in a damage region. Future work will focus on additional advantages of this framework, such as for denoising or compression of data. We will also explore other physics constraints, such as other forms of the wave equation.

ACKNOWLEDGMENTS

This work was supported through a grant #DE-NE0009392 from the Department of Energy (DOE) - Nuclear Energy (NE) program.

REFERENCES

1. Lee, S. and J. S. Popovics. 2024. "The potential for material property characterization using physics-informed neural networks and ultrasonic wave data," *Res. Nondestruct. Eval.*, 35(4):211–231.
2. Li, Y., B. Xu, Y. Zou, G. Sha, and G. Cai. 2024. "Leveraging physics-informed neural networks for wavefield analysis in laser ultrasonic testing," *Nondestruct. Test. Eval.*:1–23.
3. Shukla, K., P. C. Di Leoni, J. Blackshire, D. Sparkman, and G. E. Karniadakis. 2020. "Physics-informed neural network for ultrasound nondestructive quantification of surface breaking cracks," *J. Nondestruct. Eval.*, 39(3).
4. Cross, E. J., S. J. Gibson, M. R. Jones, D. J. Pitchforth, S. Zhang, and T. J. Rogers. 2022. "Physics-informed machine learning for structural health monitoring," in *Structural Integrity*, Springer International Publishing, pp. 347–367.
5. Rizvi, S. H. and M. Abbas. 2023. "From data to insight, enhancing structural health monitoring using physics-informed machine learning and advanced data collection methods," *Eng. Res. Express*, 5(3):1–28.
6. Cai, S., Z. Mao, Z. Wang, M. Yin, and G. E. Karniadakis. 2022. "Physics-informed neural networks (PINNs) for fluid mechanics: a review," *Acta Mech. Sin.*, 37(12):1727–1738.
7. Tetali, H. V., K. S. Alguri, and J. B. Harley. 2019. "Beyond Black-box Dictionary Learning for Waves," in *Proc. of the Machine Learning and the Physical Sciences Workshop at the Conference on Neural Information Processing Systems (NeurIPS)*, pp. 1–5.
8. Harley, J. B., B. Haeffele, and H. V. Tetali. 2024. "Unsupervised wave physics-informed representation learning for guided wavefield reconstruction," in *Dynamic Data Driven Applications Systems Conference Proceedings*, Springer Nature Switzerland, Cham, Lecture Notes in Computer Science, pp. 163–172.
9. Tetali, H. V., J. Harley, and B. Haeffele. 2023. "Wave physics-informed matrix factorizations," *IEEE Trans. Signal Process.*, 72:535–548.
10. Raissi, M., P. Perdikaris, and G. E. Karniadakis. 2019. "Physics-informed neural networks: A deep learning framework for solving forward and inverse problems involving nonlinear partial differential equations," *J. Comput. Phys.*, 378:686–707.
11. Ruzzene, M. 2007. "Frequency-wavenumber domain filtering for improved damage visualization," *Smart Mater. Struct.*, 16(6):2116–2129.
12. Michaels, T. E., M. Ruzzene, and J. E. Michaels. 2009. "Incident wave removal through frequency-wavenumber filtering of full wavefield data," *Review of Progress in Quantitative Nondestructive Evaluation*, 1096:604–611.
13. Kudela, P., M. Radzieński, and W. Ostachowicz. 2015. "Identification of cracks in thin-walled structures by means of wavenumber filtering," *Mech. Syst. Signal Process.*, 50-51:456–466.
14. Flynn, E. B., S. Y. Chong, G. J. Jarmer, and J. R. Lee. 2013. "Structural imaging through local wavenumber estimation of guided waves," *NDT and E Int.*, 59:1–10.
15. Michaels, J. E., S. J. Lee, A. J. Croxford, and P. D. Wilcox. 2013. "Chirp excitation of ultrasonic guided waves," *Ultrasonics*, 53(1):265–270.